Letter

A facile synthesis of mesoporous NiO nanosheets and their application in CO oxidation

CrossMark

A B S T R A C T

Mesoporous NiO nanosheets were prepared by a facile sol–gel process using Aerosol-OT, Bis(2-ethyl hexyl) sulfosuccinate sodium salt (AOT) as anionic surfactant. The products were analyzed by XRD, Raman spectroscopy, N_2 adsorption–desorption, FESEM and TEM studies. The morphology and textural properties of the products were tuned by using different amounts of the surfactant. TEM images exhibited nanosheets particles of thickness 80–100 nm in which nanograins (10–20 nm) were assembled. A probable mechanism was illustrated for the formation of NiO nanosheets. Catalytic activity for CO oxidation was performed with the synthesized products. The nanosheet particles obtained in the presence of 1 mmol AOT with the surface area of 88.23 $m^2 g^{-1}$ exhibited the better CO oxidation, i.e., T_{50} (50% conversion) and T_{100} (100% conversion) were at 245 °C and 288 °C, respectively.

1. Introduction

Nanocatalysts have attracted great research interest due to their significant functional properties such as high specific surface area, novel size and shape dependent properties compared to their bulk materials. These materials have potential applications in catalysis, drug delivery, electrochemistry, waste-water treatment, etc. The morphology, size, shape and surface textural properties of nanomaterials influence their optical, electronic, magnetic and catalytic properties. Transition metal oxides with varied morphology and tunable mesoporosity find possible applications in materials science and technology. Nickel (II) oxide (NiO) and nickel (II) composites in particular have attracted considerable interest because of a broad range of applications, namely magnetic materials [1,2], photo voltaics [3], batteries [4], catalysis [5], gas sensors [6], p-type transparent conducting films [7], electrochromic windows [8], waste water treatment [9], and so on. Different methods have been reported for the synthesis of NiO, such as sol–gel [10], microemulsion [11], hydrothermal [12], co-precipitation [13], sonochemical [14], microwave [15], etc.

Catalytic oxidation of CO is important in many practical applications, namely air purification, pollution control devices, CO removal in heavy industry, CO gas sensors, purification of hydrogen for proton-exchange fuel cells, etc. [16]. There are different types of oxidation catalysts which transform CO into CO_2. For oxidation catalysis, the precious metals such as Au, Pd, Ru, Pt, Ir and Rh are generally used. However, keeping in mind the cost factor, considerable efforts have been made to searching transition metal oxides for catalytic oxidation of CO. Catalytic properties for CO

oxidation have been reported by many researchers [17–19]. Morphologically controlled synthesis of NiO nanocatalyst is becoming very much significant for catalytic reactions. Various NiO nanostructures, namely nanotubes [20], nanowires [21], nanorods [22], nanoflower [23], etc. have been reported.

NiO nano-sheets were commonly synthesized by hydrothermal method [24–27]. Purushothaman et al. synthesized nanosheet-assembled NiO using sodium dodecyl sulphate (SDS) as surfactant via lamellar micelles and a self-assembly process [24]. Cheng et al. [9] prepared NiO nano-sheets by chemical precipitation method at 90 °C for 48 h followed by heat-treatment at 300 °C for 5 h. Sun et al. synthesized porous NiO nanosheets by wet-chemical methods at 80 °C using different surfactants [28] followed by calcination at different temperatures. In the present study, NiO nano-sheets were synthesized by a facile sol–gel process at room temperature (30 °C) in the presence of nickel nitrate, ethanol, water, tartaric acid, using Aerosol-OT, Bis(2-ethyl hexyl) sulfosuccinate sodium salt (AOT) as anionic surfactant, followed by calcinations at 450 °C. A tentative mechanism was proposed for the formation of NiO nano-sheets. The synthesized NiO nano-sheets were quite promising materials towards catalytic oxidation of CO to CO_2. The effect of surfactant concentration on the morphology, textural properties and catalytic performance of the samples was investigated in this work.

2. Experimental

2.1. Materials

Nickel nitrate hexahydrate ($Ni(NO_3)_2 \cdot 6H_2O$), tartaric acid, Aerosol-OT, and Bis(2-ethyl hexyl) sulfosuccinate sodium salt (AOT) were purchased from Sigma–Aldrich. Absolute ethanol was
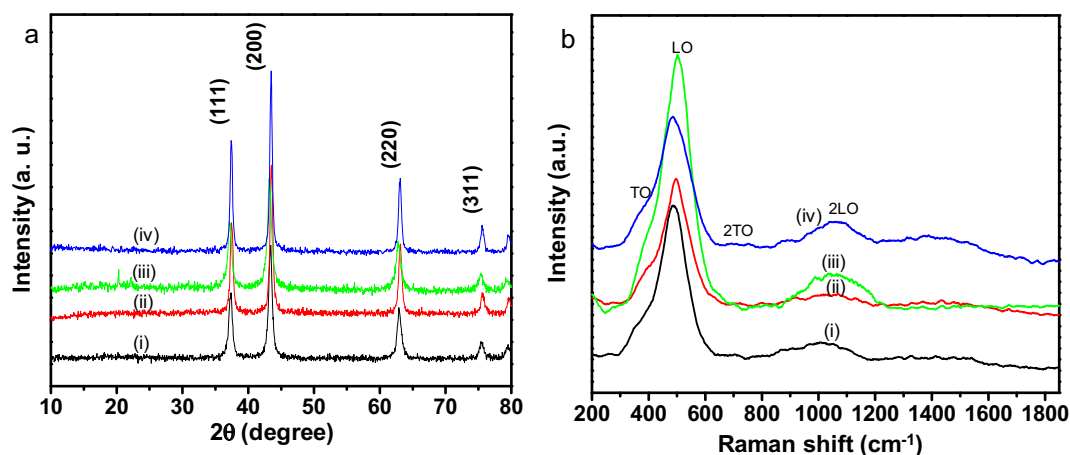
Fig. 1. (a) XRD patterns and (b) Raman spectra of NiO nanosheets for the samples: (i) NiO-0, (ii) NiO-0.5, (iii) NiO-1 and (iv) NiO-2.

purchased from Merck, Germany. Deionized (DI) water was used throughout the experiment.

2.2. Preparation of NiO nanosheets

In a typical synthesis, 10 mmol nickel nitrate hexahydrate ($Ni(NO_3)_2 \cdot 6H_2O$) was dissolved in 10 mL ethanol followed by addition of different concentrations (0, 0.5, 1 and 2 mmol) of Aerosol-OT, Bis(2-ethyl hexyl) sulfosuccinate sodium salt (AOT) solution in 30 mL water–ethanol (2:1) mixed solvent under stirring for 2 h. Then 10 mmol tartaric acid dissolved in 10 mL ethanol was added slowly to each of the above solution under stirring. With time colloidal particles started generating in solution. Stirring was continued overnight to render a greenish product. It was centrifuged and washed with water and acetone followed by drying at 60 °C. The dried products were calcined at 450 °C/2 h. The samples were designated as NiO-0, NiO-0.5, NiO-1 and NiO-2 for AOT concentrations of 0 mmol, 0.5 mmol, 1 mmol and 2 mmol, respectively.

2.3. Characterization

X-ray diffraction (XRD) studies were performed by using a Philips X'Pert Pro XRD (Model: PW 3050/60) with Ni-filtered Cu-K_α radiation ($\lambda = 0.15418$ nm), operating at 40 kV and 30 mA. The Raman spectrum was recorded using a RENISHAW spectrometer with 514 nm radiation from an argon laser at room temperature. Nitrogen adsorption and desorption measurements were performed at liquid nitrogen temperature (77 K) on a Quantachrome (ASIQ MP) instrument. The powders were outgassed in vacuum at 200 °C for 4 h prior to the measurement. The total surface area was determined by BET method. The total pore volume was estimated from the amount of nitrogen adsorbed at the relative pressure (p/p_0) of ca 0.99. The morphology of the particles was examined by field emission scanning electron microscopy, FESEM (Model: Zeiss, Supra^{TM} 35VP, Oberkochen, Germany) operating with an accelerating voltage of 10 kV, and transmission electron microscopy (TEM), using a Tecnai G2 30ST (FEI) instrument operating at 300 kV.

2.4. Catalytic oxidation of CO

The catalytic test for CO oxidation was performed in a continuous flow fixed-bed glass tubular reactor (internal diameter (i.d.) = 4 mm). 50 mg of catalyst (NiO nanosheet) was used in each experiment. Before catalytic test, the catalyst was pre-treated with a mixed gas of 90 vol% He and 10 vol% O_2 with flow rate of 40 mL min^{-1} for 30 min. After pre-treatment, a standard reaction

gas mixture containing 1 vol% CO, 20 vol% O_2 and balance with N_2 was passed through the catalyst bed at a flow rate of 40 mL min^{-1}. The weight hourly space velocity (WHSV) was 48,000 mL g^{-1} h^{-1}. The conversion of CO was measured by on-line gas chromatography equipped with a thermal conductivity detector (TCD) after the catalyst bed temperature was stabilized for 30 min to obtain a steady state. The conversion of CO to CO_2 was measured at different temperatures.

3. Results and discussion

3.1. Characterization of NiO nanosheets

3.1.1. XRD analysis

Fig. 1a shows the XRD patterns of NiO nanosheets for the samples: (i) NiO-0, (ii) NiO-0.5, (iii) NiO-1 and (iv) NiO-2. The existence of strong diffraction peaks corresponding to (111), (200), (220) and (311) crystal planes indicated the formation of phase pure cubic NiO (JCPDS 47-1049).

3.1.2. Raman analysis

The Raman spectra of NiO nanosheets: (i) NiO-0, (ii) NiO-0.5, (iii) NiO-1 and (iv) NiO-2 are shown in Fig. 1b. Four Raman peaks located at around 420, 500, 708 and 1075 cm^{-1} were observed in all the samples. The peaks at around 420 and 500 cm^{-1} were assigned to first order transverse optical (TO) and longitudinal optical (LO) phonon modes of NiO, respectively. The peaks at around 708 and 1075 cm^{-1} were attributed to the combination of 2TO and 2LO, respectively [22,23].

3.1.3. Textural properties

The textural properties of NiO nanosheets were studied by N_2 sorption analysis. Fig. 2a shows N_2 adsorption–desorption isotherms of NiO nanosheets for the samples: (i) NiO-0, (ii) NiO-0.5, (iii) NiO-1 and (iv) NiO-2. It displays IUPAC type IV isotherms with H3 type hysteresis. It indicated plate-like mesoporosity in the samples [29]. The BET surface area was found to be 32.9, 63.8, 88.2 and 62.6 m^2 g^{-1} for the sample, NiO-0, NiO-0.5, NiO-1 and NiO-2, respectively accompanying with corresponding pore volumes of 0.17, 0.28, 0.27 and 0.16 cm^3 g^{-1}, respectively. It indicated that 1 mmol AOT was an optimum concentration to render maximum surface area followed by significant decrease in surface area and pore volume with increase in AOT concentration to 2 mmol. The BJH pore size distributions derived from desorption data of the corresponding isotherms are shown in Fig. 2b. It indicated narrow pore size distributions centred at around 3.7 nm for all the samples.
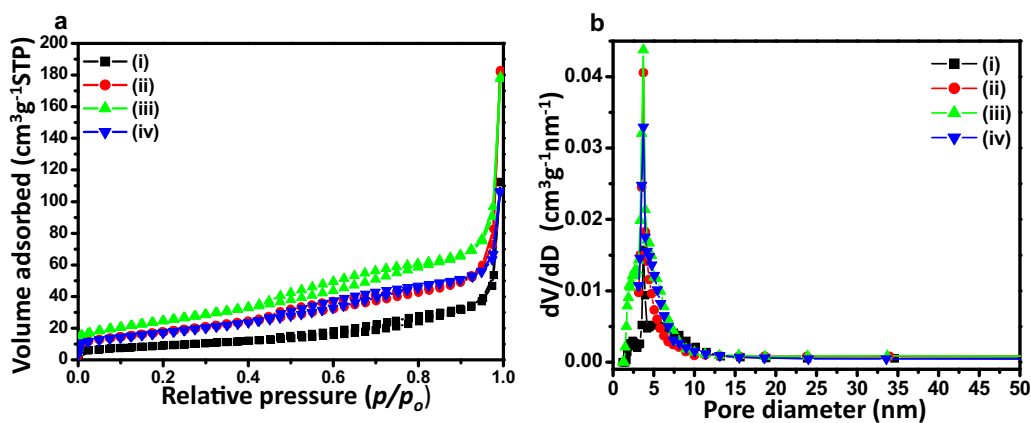
Fig. 2. (a) N$_2$ adsorption–desorption isotherms of NiO for the samples: (i) NiO-0, (ii) NiO-0.5, (iii) NiO-1 and (iv) NiO-2, and (b) the corresponding pore size distributions evolved from BJH desorption isotherms.
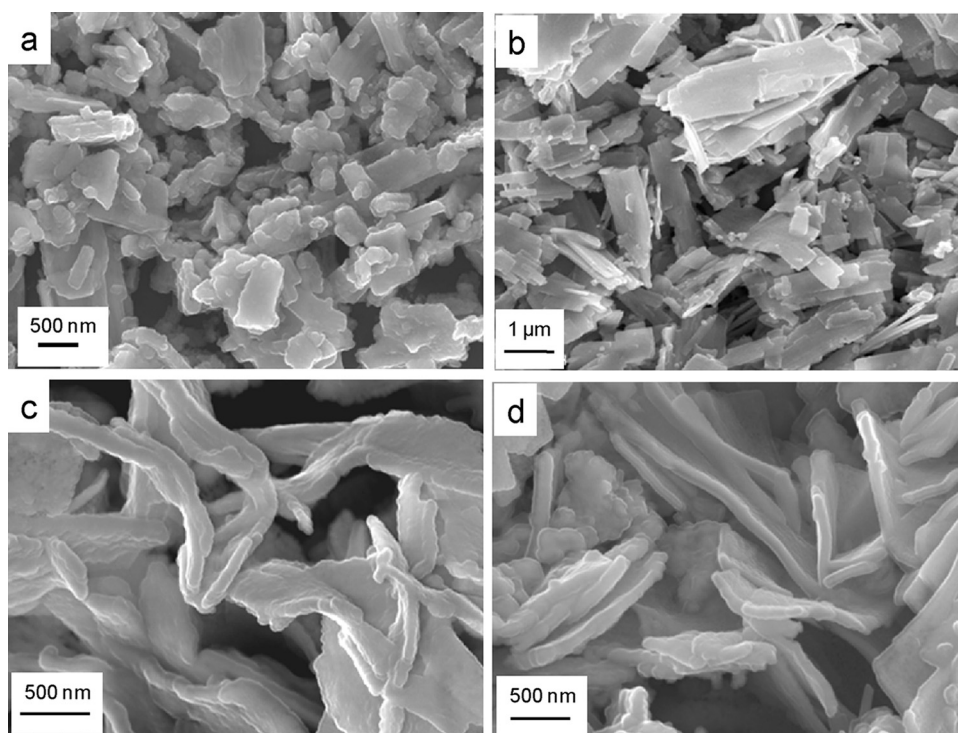

Fig. 3. FESEM images of the samples: (a) NiO-0, (b) NiO-0.5, (c) NiO-1 and (d) NiO-2.

3.1.4. Microstructural studies

Fig. 3 shows the FESEM microstructures for the samples: (a) NiO-0, (b) NiO-0.5, (c) NiO-1 and (d) NiO-2. It revealed that sheet-like NiO particles started growing in the presence of the anionic surfactant AOT, which became more pronounced for 1–2 mmol AOT concentration. The nano-sheet-like particles in the presence of AOT were clearly confirmed by TEM images (Fig. 4a–d). In the absence of AOT, sheet-like particles were not obtained (Fig. 4a), while it was revealed in the presence of 0.5, 1 and 2 mmol AOT (Fig. 4b–d). It is worth mentioning that AOT played an important role in the formation of nano-sheet-like particles. From TEM images, it is clear that the thickness of sheets were 80–100 nm in which nanograins (10–20 nm) were assembled resulting porosity between the component subunits. The microstructures of the corresponding samples were further studied by high resolution TEM (HRTEM) (Fig. 4e–h); the insets show the selected area electron diffraction (SAED) of the corresponding samples. The lattice spacing of 0.21 nm

corresponded to the (200) plane of cubic NiO. The SAED image shows the polycrystalline nature of the particles.

3.1.5. Formation mechanism for NiO nano-sheet

We have illustrated a tentative mechanism for the formation of NiO nano-sheets (Fig. 5). The anionic surfactant, Bis(2-ethyl hexyl) sulfosuccinate sodium salt (AOT) (hydrophilic-lypophilic balance (HLB) = 10.2) in the presence of water, and ethanol as cosurfactant [30] forms lamellar micelles [24]. In the presence of nickel nitrate in aqueous solution, the Ni^{2+} ions interact with the hydrophilic head group of anionic surfactant (AOT) and non-ionic cosurfactant (ethanol) in lamellar micelles structure. With the progress of reaction under stirring condition, the Ni^{2+} ions in lamellar micelles interact with tartaric acid molecules forming sheet-like self-assembled architectures in which the organo-nickel particles are oriented together in sheet-like structure. After
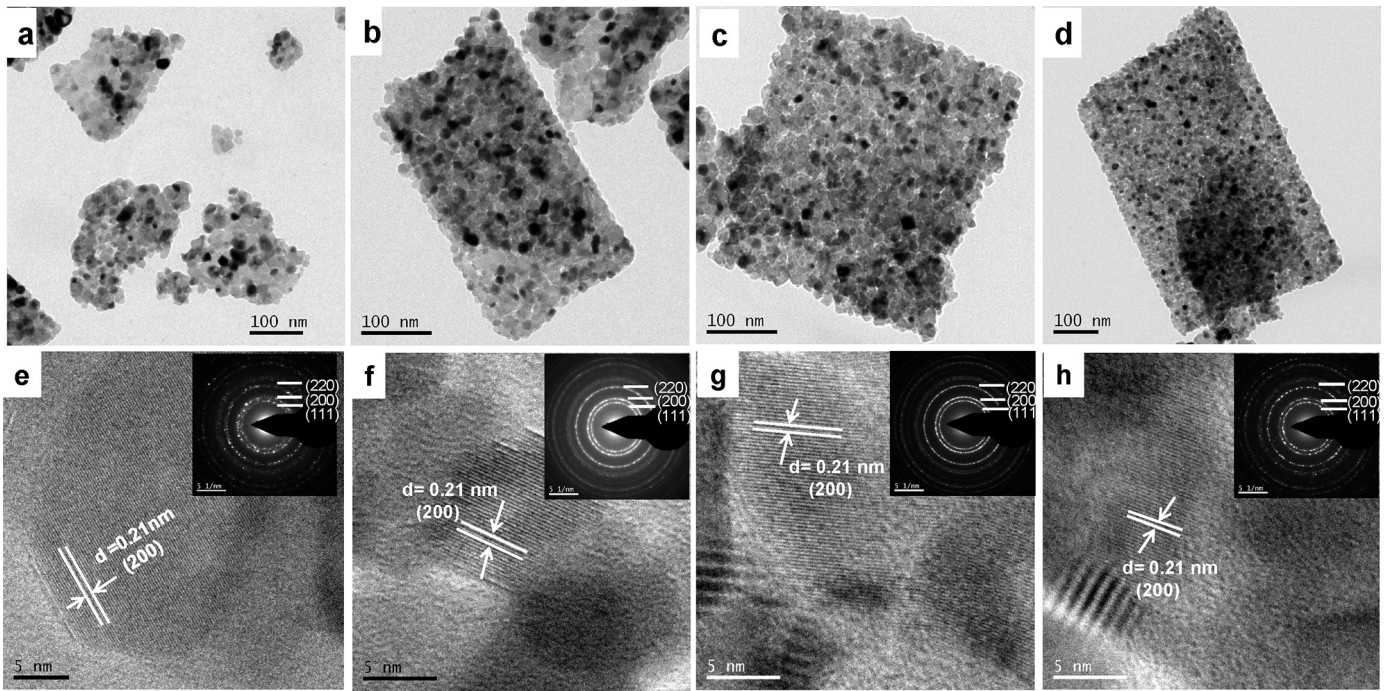
Fig. 4. TEM images of the samples: (a) NiO-0, (b) NiO-0.5, (c) NiO-1 and (d) NiO-2, and their corresponding HRTEM images (e–h) (insets shows corresponding SAED patterns).

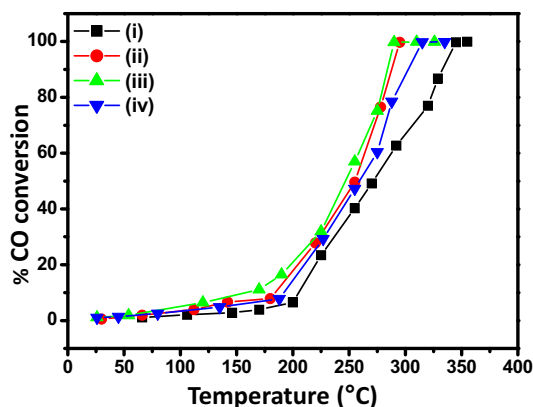**Fig. 5.** Schematic illustration for the formation of NiO nano-sheets.

Fig. 6. Catalytic activity of CO oxidation under different reaction temperatures for the samples: (i) NiO-0, (ii) NiO-0.5, (iii) NiO-1 and (iv) NiO-2.

washing and calcination, the surfactant molecules and organic moieties are removed forming NiO nanosheets.

3.1.6. Catalytic oxidation of CO

Fig. 6 shows the catalytic performance of NiO nanosheets for CO oxidation. It is clear that catalytic activity increased in the order of NiO-0 < NiO-2 < NiO-0.5 < NiO-1. The 50% CO conversion (T_{50}) occurred at around 273 °C, 255 °C, 245 °C and 258 °C for the samples, NiO-0, NiO-0.5, NiO-1 and NiO-2, respectively, while 100% CO conversion (T_{100}) of the corresponding samples took place at around 345 °C, 295 °C, 288 °C and 314 °C, respectively. The morphology and textural properties of the samples played an important role for variation of CO oxidation. The maximum catalytic efficiency of the sample, NiO-1 was due to its nanosheet architecture and higher surface area. Interestingly, instead of better nanosheet structure of the sample, NiO-2 compared to that of the sample, NiO-0.5, and having comparable surface area, the former rendered less catalytic performance than the latter sample. This could be explained due to higher pore volume of NiO-0.5 than that of NiO-2. In the absence of AOT, the least CO oxidation of NiO-0 was due to minimum surface area, pore volume, and the absence of nanosheet-like structure. The porous nanosheet structure possessed better exposed surface suitable for active sites for adsorption of reactants in catalytic reaction.

4. Conclusion

Mesoporous NiO nanosheets were synthesized by a facile sol–gel method. The morphology and textural properties were tuned by using different amount of anionic surfactant, AOT. With increasing AOT concentration, better nanosheet morphology was obtained. The optimum concentration of 1 mmol AOT rendered maximum surface area. The catalytic performance of NiO nanosheet for CO oxidation was affected by the morphology as well as surface textural properties of the catalyst. This work provides a new direction to study other morphologically tuned porous transition metal oxides towards CO oxidation.

Acknowledgements

References

[1] H. Pang, Q. Lu, Y. Lee and F. Gao, Chem. Commun., 7542–7544 (2009).
[2] R. Kurosawaa, T. Suzukia, T. Nakayamaa, H. Suematsua, K. Niiharaa, S. Satokawab, Y. Yasukawac and X.L. Extreme, J. Asian Ceram. Soc. 41–43 (2014).
[3] E.L. Ratcliff, J. Meyer, K.X. Steirer, A. Garcia, J.J. Berry, D.S. Ginley, D.C. Olson, A. Kahn and N.R. Armstrong, Chem. Mater., 23, 4988–5000 (2011).
[4] B. Varghese, M.V. Reddy, Z. Yanwu, C.S. Lit, T.C. Hoong, G.V. Subba Rao, B.V.R. Chowdari,.T.S.A. Wee, C.T. Lim and C.-H. Sow, Chem. Mater., 20, 3360–3367 (2008).
[5] C.-C. Hu and H. Teng, J. Catal., 272, 1–8 (2010).
[6] I. Hotovya, V. Rehaceka, P. Sicilianob, S. Caponec and L. Spiessd, Thin Solid Films, 418, 9–15 (2002).
[7] C.W. Kim, Y.S. Son, A.U. Pawar, M.J. Kang, J.Y. Zheng, V. Sharma and P. Mohanty, J. Mater. Chem. A, 2, 19867–19872 (2014).
[8] G.-F. Cai, J.-P. Tu, J. Zhang, Y.-J. Mai, Y. Lu, C.-D. Gu and X.-L. Wang, Nanoscale, 4, 5724–5730 (2012).
[9] B. Cheng, Y. Le, W. Cai and J. Yu, J. Hazard. Mater., 185, 889–897 (2011).
[10] S. Pilban Jahromia, N.M. Huang, M.R. Muhamad and H.N. Lim, Ceram. Int., 39, 3909–3914 (2013).
[11] T. Ahmad, K.V. Ramanujachary, S.E. Lofland and A.K. Ganguli, Solid State Sci., 8, 425–430 (2006).
[12] M.-G. Ma, J.-F. Zhu, J.-X. Jiang and R.-C. Sun, Mater. Lett., 63, 1791–1793 (2009).
[13] X. Xin, Z. Lu, B. Zhou, X. Huang, R. Zhu, X. Sha, Y. Zhang and W. Su, J. Alloys Compd., 427, 251–255 (2007).
[14] A. Aslani, V. Oroojpour and M. Fallahi, Appl. Surf. Sci., 257, 4056–4061 (2011).
[15] S.K. Meher, P. Justin and G. Ranga Rao, ACS Appl. Mater. Interfaces, 3, 2063–2073 (2011).
[16] S. Paldey, S. Gedevanishvili, W. Zhang and R. Rasouli, Appl. Catal. B, 56, 241–250 (2005).
[17] D. Wang, R. Xu, X. Wang and Y. Li, Nanotechnology, 17, 979–983 (2006).
[18] J. Zhu, Z. Gui, Y. Ding, Z. Wang, Y. Hu and M. Zou, J. Phys. Chem. C, 111, 5622–5627 (2007).
[19] D.N. Nhiema, L.M. Daia, N.D. Van and D.T. Limb, Ceram. Int., 39, 3381–3385 (2013).
[20] H. Pang, Q. Lu, Y. Li and F. Gao, Chem. Commun., 7542–7544 (2009).
[21] Q. Yang, J. Sha, X. Ma and D. Yang, Mater. Lett., 59, 1967–1970 (2005).
[22] W. Wang, Y. Liu, C. Xu, C. Zheng and G. Wang, Chem. Phys. Lett., 362, 119–122 (2002).
[23] L.X. Song, Z.K. Yang, Y. Teng, J. Xia and P. Du, J. Mater. Chem. A, 1, 8731–8736 (2013).
[24] K.K. Purushothaman, I.M. Babu, B. Sethuraman and G. Muralidharan, ACS Appl. Mater. Interfaces, 5, 10767–10773 (2013).
[25] J. Hu, K. Zhu, L. Chen, H. Yang, Z. Li, A. Suchopar and R. Richards, Adv. Mater., 20, 267–271 (2008).
[26] C. Li and S. Liu, J. Nanomater., 2012, 1–6 (2012).
[27] Y. Yao, J. Zhang, Z. Wei and A. Yu, Int. J. Electrochem. Sci., 7, 1433–1442 (2012).
[28] X. Sun, G. Wang, J.Y. Hwang and J. Lian, J. Mater. Chem., 21, 16581–16588 (2011).
[29] M. Roy, S. Ghosh and M.K. Naskar, Mater. Chem. Phys., 159, 101–106 (2015).
[30] C.S. Chauhan and N.S. Chouhan, Int. J. Adv. Res. Pharm. Biosci., 2, 320–325 (2012).

Pallab Bose
Sourav Ghosh
Somjyoti Basak
Milan Kanti Naskar*
Sol-Gel Division, CSIR-Central Glass and Ceramic Research Institute, Kolkata 700032, India

* Corresponding author.
Tel.: +91 3324733496x3516.
E-mail address: milan@cgcri.res.in (M.K. Naskar)